Eur. J. Mineral.
2003, **15**, 803-814

This paper was presented at the EMPG IX
meeting in Zurich, Switzerland (March 2002)

Water solubility in haplobasaltic melts

DARJA BENNE* and HARALD BEHRENS

Institut für Mineralogie, Universität Hannover, Welfengarten 1, D-30167 Hannover, Germany

Abstract: The solubility of water in melts of the haplobasaltic system ($NaAlSi_3O_8$-$CaAl_2Si_2O_8$-$CaMgSi_2O_6$, Ab-An-Di) was investigated at pressures of 50, 200 and 500 MPa and at temperatures between 1200°C and 1420°C using an internally heated gas pressure vessel. Compositions close to the binary joins Ab_{100}-An_{100} and $Ab_{50}Di_{50}$-$An_{50}Di_{50}$ were studied. The water content of the glasses was analysed using Karl-Fischer-titration and near-infrared (NIR) spectroscopy. Linear molar absorption coefficients for the NIR combination bands of OH groups at 4500 cm^{-1} (ε_{OH}) and molecular H_2O at 5200 cm^{-1} (ε_{H2O}) were determined for $Ab_{50}An_{50}$, $An_{56}Di_{44}$, and $Ab_{54}Di_{46}$ compositions. Concentration of OH groups is found to be significantly higher in $Ab_{50}An_{50}$ glasses than in other glasses quenched at similar rate. This is attributed to the depolymerisation of the network structure enabling the formation of stable Ca-complexes in the glasses.

An increase in pressure from 50 to 200 or from 200 to 500 MPa approximately doubles the water solubility in haplobasaltic melts. Depending on compositions 2.0-3.0 wt% water can be dissolved at 50 MPa, 3.7-6.1 wt% at 200 MPa and 7.6-12.4 wt% at 500 MPa. In general, the lowest H_2O solubility was found in the $An_{56}Di_{44}$ melt. At 50 MPa, the variation of water solubility with composition appears to be complex but the precision of the data does not allow to extract reliably compositional trends. In general, data at 200 and 500 MPa show a strong decrease in H_2O solubility with increasing Di content, *e.g.* from 5.99 wt% (Ab_{100}) to 4.94 wt% ($Ab_{54}Di_{46}$) and from 5.81 wt% ($Ab_{50}An_{50}$) to 5.21 wt% ($Ab_{27}An_{29}Di_{44}$) at 1200°C/200 MPa. The effect of Ab/An ratio on water solubility appears to be small at 200 MPa. In contrast, at 500 MPa the water solubility decreases strongly with increasing An content of the melt.

Key-words: water solubility, haplobasaltic melts, Karl-Fischer titration, IR spectroscopy, H_2O speciation.

1. Introduction

In nearly all melting processes of silicates in the Earth's crust and mantle fluid components are of great importance, in particular H_2O. Even small amounts of dissolved water decrease the solidus and the liquidus temperatures of magmas by several tens to hundreds degrees Kelvin and reduce the viscosity of the magma by several orders of magnitude. Therefore, water solubility data and knowledge of the incorporation mechanisms of H_2O in silicate melts are of great interest in geosciences.

The present study focuses on the effect of melt composition on the solubility of H_2O in haplobasaltic melts (Di-Ab-An, $CaMgSi_2O_6$-$NaAlSi_3O_8$-$CaAl_2Si_2O_8$). The variation of water solubility with melt composition was investigated at different pressures and temperatures. The results can be used as a basis for development of models for the generation and the evolution of basaltic magmas, as it was done successfully for granitic magmas (Johannes & Holtz, 1996).

A by-product of our work was the investigation on the water speciation in haplobasaltic glasses. H_2O dissolves in silicate glasses and melts in at least two forms: H_2O molecules and OH groups. Infrared spectroscopy (IR) is a powerful analytical tool to determine the concentration of both hydrous species (Stolper, 1982). For quantitative evaluation of the spectra, the molar absorption coefficients for the absorption bands must be known. These absorption coefficients are strongly dependent on the anhydrous glass composition (Silver *et al.*, 1990; Behrens *et al.*, 1996). We established new calibrations of the absorption coefficients for three compositions in the haplobasaltic system. The OH- and H_2O-contents in the glasses were frozen at the glass-transition and thus do not represent equilibrium concentrations in melts at high temperature (Dingwell & Webb, 1990). *In situ* analyses have shown that with increasing temperature the formation of hydroxyl groups is favoured (Nowak & Behrens, 1995, 2001; Shen & Keppler, 1995). Although the water speciation in the glasses does not allow direct conclusions about speciation in the melts at high temperature, there are nevertheless implications for the speciation at the glass transition and for the incorporation mechanism of water in silicate glasses and melts.

*Corresponding author. Present address: Otto-Schott-Institut für Glaschemie, Universität Jena, Fraunhoferstr. 6, D-07743 Jena, Germany. E-mail: darja.benne@uni-jena.de

DOI: 10.1127/0935-1221/2003/0015-0803

0935-1221/03/0015-0803 $ 5.40

Table 1. Composition of glasses (in wt.%).

Sample	Ab_{100}	$Ab_{65}An_{35}$ [a]	$Ab_{50}An_{50}$ [b]	An_{100}	$Ab_{54}Di_{46}$	$Ab_{27}An_{29}Di_{44}$	$An_{56}Di_{44}$
SiO_2	69.19	56.36	55.20	42.05	62.82	54.19	48.82
Al_2O_3	18.83	23.31	28.24	36.63	10.65	15.88	21.00
MgO	-	-	-	0.11	8.17	8.07	7.45
CaO	-	6.77	10.59	20.48	12.89	18.16	23.41
Na_2O	11.96	6.98	5.75	0.22	6.40	3.03	0.07
K_2O	0.02	0.03	-	0.02	-	-	-
Σ	99.98	93.45	99.82	99.49	100.92	99.37	100.75

Measurement conditions: CAMECA Camebax microprobe, acceleration voltage 15 kV, beam current 18 nA, beam diameter 20-30 µm. [a]) The composition of the $Ab_{65}An_{35}$ glass was determined using the hydrous glass of the 1200°C, 200 MPa run. The low total of the microprobe analysis is due to dissolved H_2O (5.61 wt%). [b]) Analysis of $Ab_{50}An_{50}$ glasses by the Schott company for SiO_2 and Al_2O_3 using spectro-photometry and for MgO, CaO, Na_2O, K_2O atomic absorption spectrometry.

2. Experimental

2.1 Starting materials

The investigated melt compositions belong to two binary joins of the ternary system Di-Ab-An: (1) the plagioclase join Ab-An and (2) the plagioclase/diopside 1:1 join $Ab_{50}Di_{50}$-$An_{50}Di_{50}$ (nominal compositions in wt%). Anhydrous glasses were used as starting materials. The Di-bearing compositions were synthesised using mixtures of oxides and carbonates. Each mixture was decarbonated at 1000°C for 1 h in a platinum crucible before heating to 1600°C. After melting for 4 h at 1600°C, the melt was quenched to glass by setting the hot crucible into a water bath. Glasses with compositions $Ab_{50}An_{50}$, $Ab_{80}An_{20}$, Ab_{100} and An_{100} were synthesised by the Schott Company (Mainz, Germany). The $Ab_{65}An_{35}$ glass was prepared by melting an appropriate powder mixture of the Ab and the $Ab_{50}An_{50}$ glass. Chemical compositions of the glasses are given in Table 1.

2.2 Experimental procedures

Rectangular glass blocks (typical size 5 * 2 * 2 mm) and doubly distilled water were sealed by welding into platinum capsules. The amount of added water was slightly higher than the expected solubility value. Capsules were cooled with liquid nitrogen during sealing to avoid water loss. The sealed capsules were checked for leaks by testing for weight loss after annealing at 105°C for at least 1 h.

All experiments were performed in a vertically internally heated pressure vessel (IHPV) pressurised with Argon. A detailed description of the technique is given by Behrens *et al.* (2001). Rapid quench experiments were performed using a set-up similar to that used by Roux & Lefèvre (1992).

Different sets of experiments were performed with run duration ranging from 15 to 72 h, at 50 to 500 MPa and 1200 to 1420°C; for a detailed description see Table 2. Initial cooling rates for runs terminated with a normal quench (*i.e.* by switching off the power supply) were ~ 200°C/min decreasing to ~ 100°C/min near the glass transition of hydrous glasses (300-600°C). In drop quench experiments, cooling rates were determined to be ~ 150°C/s using the geospedometer of Zhang *et al.* (2000), which is based on water speciation in hydrous rhyolitic glasses.

Between 4 to 6 capsules were simultaneously run in each experiment. Because the pressure was identical for all of these capsules, even small differences in water solubility could be reliably resolved. Temperature has only a minor influence on water solubility at the P-T conditions used in our study (Behrens *et al.*, 2001). We suggest that small differences in the temperature arising from the presence of a thermal gradient across the charges (always less than 10°C per cm) do not noticeably affect on conclusions about the compositional dependence of water solubility.

3. Analytical procedures

3.1 Densities

The densities of the glasses must be known for quantification of water species and total water by IR absorption spectroscopy (Stolper, 1982). Densities were determined by weighing single glass chips (20-30 mg) in air and in water. Due to the small size of the run products, the uncertainty of the determination is relatively high (1-3 %).

3.2 Karl-Fischer-Titration (KFT)

Water concentrations of the glasses were determined by pyrolysis and subsequent KFT (Behrens *et al.*, 1996). Glasses with a water content > 3 wt.% dehydrate explosively, leading to a sputtering of the glass pieces out of the heating zone. Thus, the glasses were tightly wrapped into platinum foils. Behrens (1995) has shown that residual water contents in polymerised aluminosilicate glasses after KFT are in the range of 0.10 ± 0.05 wt%. However, for more depolymerised melts of dacitic and andesitic compositions Ohlhorst *et al.* (2001) found that the amount of unextracted water is much smaller (0.02 ± 0.02 wt% H_2O). For the polymerised Ab-An melts and the more depolymerised Di-bearing melts we added 0.10 and 0.02 wt% H_2O, respectively, to the values obtained from KFT in order to account for unextracted water. The uncertainty of the KFT analysis was calculated on the basis of the uncertainty of the titration rate (± 0.02 $\mu g s^{-1}$) (Behrens *et al.*, 1996).

3.3 IR-spectroscopy

IR spectroscopy was used to check the homogeneity of water distribution in the glasses and to test the internal consistency of the solubility data for each composition, *i.e.* it was verified whether outliers from KFT measurements were due to analytical errors or to real variations in water solubility. Doubly polished glass wafers with thickness of 0.2-0.5 mm were prepared. The thickness of the sections were measured using a digital micrometer (Mitutoyo) with an uncertainty of 2 µm. The spectra were recorded using an

Table 2. Water solubility data.

Composition	P	T	Time	Type of	wt% H_2O	wt% H_2O in the glasses by KFT	Remarks	H_2O solubility
	(MPa)	(°C)	(h)	Quench	added			(wt.%)
Ab_{100}	50	1200	46	NQ	n.d.	2.54(14)		2.64
Ab_{100} *)	50	1200	48	NQ	4.5	2.59(15)		2.69
Ab_{100} *)	50	1300	48	NQ	5	2.36(15)		2.46
Ab_{100}	53	1420[b]	34	RQ	5.8	2.49(19)	2.34 wt% by NIR	2.34
Ab_{100} *)	52	1420	20	RQ	7	2.19(15)		2.29
Ab_{100}	200	1200	48	NQ	10.3	5.83(13)		5.93
Ab_{100}	200	1200	48	NQ	7	5.89(22)		5.99
Ab_{100}	200	1280	31	NQ	10	5.98(20)		6.08
Ab_{100}	200	1345[a]	15	RQ	10	5.69(15)		5.79
Ab_{100}	200	1350	15	RQ	12.2	6.41(10)	5.58 wt% by NIR	5.58
Ab_{100}	500	1200	48	NQ	n.d.	11.89(13)		11.99
Ab_{100}	500	1200	48	NQ	n.d.	12.30(13)		12.40
Ab_{100}	500	1330	19	RQ	20.6	11.23(10)	quench bubbles	>>11.33
$Ab_{65}An_{35}$	200	1200	72	NQ	n.d.	5.51(08)		5.61
$Ab_{65}An_{35}$	500	1200	48	NQ	n.d.	10.84(08)		10.94
$Ab_{50}An_{50}$	50	1200	48	NQ	7.7	-	crystals	-
$Ab_{50}An_{50}$	50	1300	48	NQ	5	2.57(17)		2.67
$Ab_{50}An_{50}$	52	1420[a]	20	RQ	5.6	2.25(13)		2.35
$Ab_{50}An_{50}$	200	1200	48	NQ	n.d.	5.71(18)		5.81
$Ab_{50}An_{50}$	200	1351	15	RQ	16.5	5.13(18)		5.23
$Ab_{50}An_{50}$	500	1200	48	NQ	n.d.	10.09(13)		10.19
$Ab_{50}An_{50}$	500	1320	18	RQ	22.5	10.38(10)		10.48
An_{100}	52	1420[a]	20	RQ	6.3	-	crystals	-
An_{100}	200	1351	15	RQ	15.1	3.56(11)		3.66
An_{100}	500	1320	18	RQ	20.6	8.87(10)		8.97
$Ab_{54}Di_{46}$	50	1200	48	NQ	4.7	-	dull	-
$Ab_{54}Di_{46}$	50	1300	48	NQ	5	2.53(14)		2.55
$Ab_{54}Di_{46}$	52	1420[a]	20	RQ	5.9	2.02(13)		2.04
$Ab_{54}Di_{46}$	200	1200	48	NQ	4.8	4.92(15)		4.94
$Ab_{54}Di_{46}$	200	1358	15	RQ	8.9	5.34(11)		5.36
$Ab_{54}Di_{46}$	500	1200	48	NQ	19.3	8.61(17)	milky	8.63
$Ab_{54}Di_{46}$	500	1310	18	RQ	20.5	10.81(10)	milky/ dull	10.83
$Ab_{27}An_{29}Di_{44}$	50	1200	48	NQ	5	2.40(15)		2.42
$Ab_{27}An_{29}Di_{44}$	50	1300	48	NQ	5	2.48(16)		2.50
$Ab_{27}An_{29}Di_{44}$	52	1420[a]	20	RQ	5.7	2.93(11)		2.95
$Ab_{27}An_{29}Di_{44}$	200	1200	48	NQ	9.4	5.19(18)		5.21
$Ab_{27}An_{29}Di_{44}$	200	1351	15	RQ	7.8	4.80(13)		4.82
$Ab_{27}An_{29}Di_{44}$	500	1200	48	NQ	24.3	8.76(18)		8.78
$Ab_{27}An_{29}Di_{44}$	500	1300	18	RQ	20.6	8.93(10)	milky	8.95
$An_{56}Di_{44}$	50	1200	48	NQ	4.5	-	crystals	-
$An_{56}Di_{44}$	50	1300	48	NQ	4.3	2.21(21)		2.23
$An_{56}Di_{44}$	52	1420[a]	20	RQ	5.5	1.98(12)		2.00
$An_{56}Di_{44}$	200	1200	48	NQ	12.6	5.27(21)		5.29
$An_{56}Di_{44}$	200	1358	15	RQ	13.2	4.28(16)	5.26 wt% by NIR	5.26
$An_{56}Di_{44}$	500	1200	48	NQ	28.6	7.57(32)		7.59
$An_{56}Di_{44}$	500	1300	18	RQ	18.3	8.00(11)	few bubbles	8.02

Notes: Water content of glasses measured by KFT are not corrected for residual water in the glasses after analysis. Errors of KFT data given in parenthesis are based on an uncertainty of 0.02 µg/s in the titration rate. Preferred data are given for the H_2O solubility in the last column. *) Data from Behrens *et al.* (2001). a) temperature oscillation of ± 10°C during run. b) temperature oscillation of ± 20°C during run. Quenching: NQ = normal quench at initial rate of *ca*. 200 °C/min, RQ = rapid quench at rate of *ca.* 150°C in the range of glass transition.

IR microscope (A590) attached to a Bruker IFS88 FTIR spectrometer. Measurement conditions were: a halogen light source, a CaF_2-beamsplitter and a narrow band MCT detector. The analysed spots were on average 30-50 µm in diameter. 50-100 scans were accumulated for each spectrum with a spectral resolution of 4 cm^{-1}.

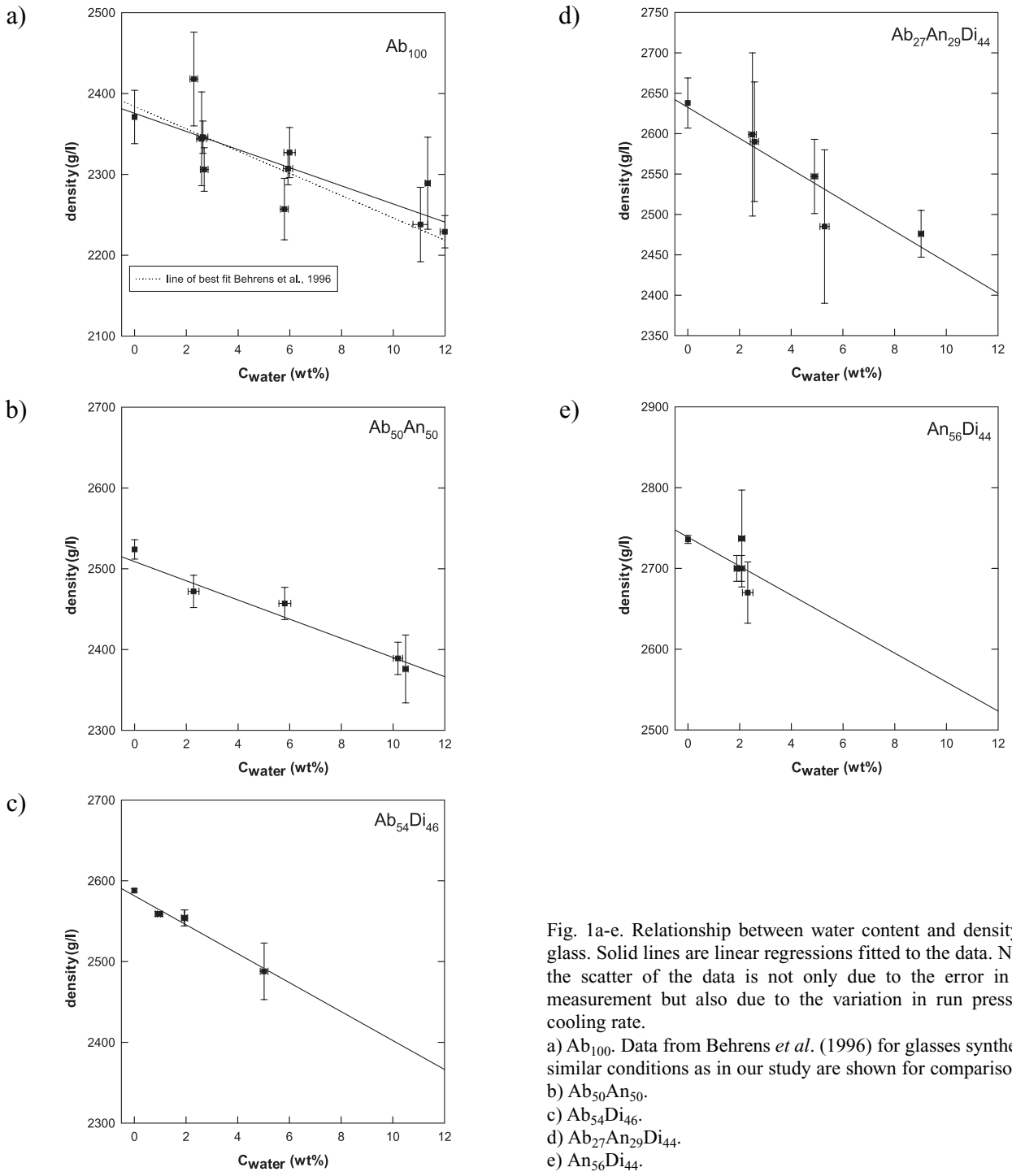

Fig. 1a-e. Relationship between water content and density of the glass. Solid lines are linear regressions fitted to the data. Note, that the scatter of the data is not only due to the error in density measurement but also due to the variation in run pressure and cooling rate.
a) Ab_{100}. Data from Behrens *et al*. (1996) for glasses synthesised at similar conditions as in our study are shown for comparison.
b) $Ab_{50}An_{50}$.
c) $Ab_{54}Di_{46}$.
d) $Ab_{27}An_{29}Di_{44}$.
e) $An_{56}Di_{44}$.

4. Results

4.1 Run products

A complete list of all runs is given in Table 2. The majority of the run products contain crystal free and bubble free glasses. In many of the capsules a free water liquid was present after the experiment as shown by drops of H_2O upon capsule opening. Further evidence for excess water during the experiment is given by liquid imprints on the surface of some of the glasses (Burnham & Jahns, 1962). In the other runs the measured water content in the glass was always much lower than the initially added water.

The experiments at 1200°C generated the most problems due to crystallisation. At this temperature, the compositions $An_{56}Di_{44}$, $Ab_{54}Di_{46}$ and $Ab_{50}An_{50}$ at 50 MPa, $Ab_{50}An_{50}$ at 200 MPa and $Ab_{27}An_{29}Di_{44}$ at 500 MPa were partially or completely crystallised. In the low pressure

runs the liquidus temperature was probably not reached (Morse, 1980). In the experiment with $Ab_{27}An_{29}Di_{44}$ at 500 MPa the amount of water in the capsule was possibly too low due to water loss during welding of the capsule. Crystal-bearing charges were not considered in this study.

Some compositions could not be quenched to clear glasses at 500 MPa from temperatures > 1300°C (Ab_{100} at 1330°C, $Ab_{54}Di_{46}$ and $Ab_{27}An_{29}Di_{44}$ at 1300°C) even when using a rapid quench. We attribute the appearance of quench bubbles in the glasses to a strong positive temperature dependence of the H_2O solubility at these conditions.

4.2 Densities

In accordance to previous work (Richet *et al*., 2000), our density data are described on best by a linear relationship between density and water content of the glasses (Fig. 1 a-e). Using the data given in Table 3 the following equations were obtained by linear regressions:

$$\rho = -19.2(\pm5.7)\cdot c_{water} + 2633(\pm31) \text{ for } Ab_{27}An_{29}Di_{44} \quad (4\text{-}1)$$

$$\rho = -17.9(\pm14)\cdot c_{water} + 2739(\pm26) \text{ for } An_{56}Di_{44} \quad (4\text{-}2)$$

$$\rho = -17.9(\pm2.3)\cdot c_{water} + 2581(\pm6) \text{ for } Ab_{54}Di_{46} \quad (4\text{-}3)$$

$$\rho = -11.9(\pm2.2)\cdot c_{water} + 2509(\pm18) \text{ for } Ab_{50}An_{50} \quad (4\text{-}4)$$

where ρ is the density in g/l and c_{water} is the total water content in wt%. The regressions represent samples with different cooling rates and run pressures. Thus, the scatter of the data not only reflects the measurement error but also real differences in density. This may explain the deviation of some Ab_{100} glasses from the linear trend obtained by Behrens *et al.* (1996) (Fig. 1a).

4.3 Analysis of the IR-spectra

Figure 2 shows the IR spectra of glasses with different bulk compositions but similar water contents (2.3-2.7 wt%). In the range of 3700-5500 cm^{-1} three absorption bands related to dissolved water are visible. The peak at 4000 cm^{-1} is an unassigned band correlated with the total water content (Stolper, 1982; Withers & Behrens, 1999). The absorption bands at 5200 cm^{-1} and 4500 cm^{-1} are assigned to the H_2O molecules and to OH groups bonded to tetrahedral cations, respectively (Scholze, 1960; Stolper, 1982). Using the peaks at 5200 cm^{-1} and 4500 cm^{-1} the concentration of molecular H_2O and OH in glasses can be determined quantitatively.

4.3.1 Positions of peak maxima

The peak positions of the OH and H_2O combination bands shift continuously towards lower wavenumbers with increasing An content at constant Di content and with increasing Di content at constant Ab/An ratio (see Fig. 2 and Table 3). In addition, the positions of the peak maxima shift slightly with increasing water content towards smaller wave numbers (see Table 3). However, this effect is only significant when the variation in water content is large and it is predominant for the 4500 cm^{-1} band.

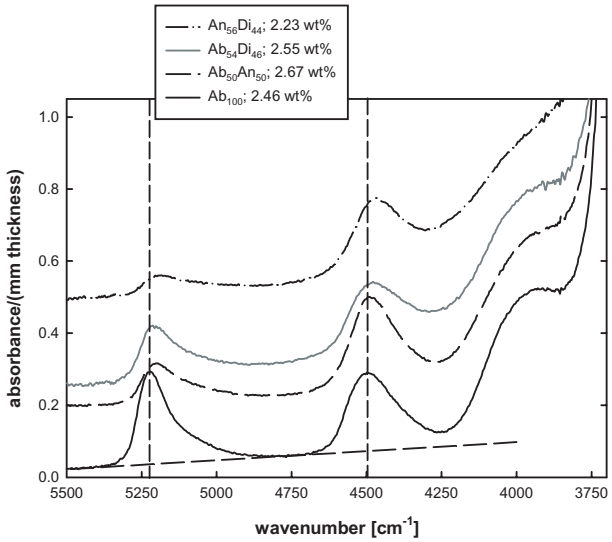

Fig. 2. Comparison of NIR absorption spectra of haplobasaltic glasses with similar total water content but different anhydrous composition. The vertical lines show the positions of the maxima of the OH combination (at 4500 cm^{-1}) and the H_2O combination band (at 5220 cm^{-1}) for the Ab_{100} glass. The baseline is illustrated for the spectrum on bottom.

4.3.2 Baseline correction

For quantifying peak heights and peak areas, an appropriate baseline under the bands at 4500 and 5200 cm^{-1} must be defined. Different procedures for baseline correction and intensity measurement were tested by Withers & Behrens (1999) and Ohlhorst *et al.* (2001). In terms of total water contents the reproducibility is very high for all of these methods but concentrations of water species may differ by more than 20 %. In this study we used a simple straight line fitted to the base of the peak at 5200 cm^{-1} and extrapolated below the 4500 cm^{-1} band (Fig. 2). This baseline was successfully applied in previous studies of our group (*e.g*., Nowak & Behrens, 1995; Behrens *et al*., 1996; Withers & Behrens, 1999; Ohlhorst *et al*., 2001) often in combination with a gaussian fitted to the band at 4000 cm^{-1} to quantify the peak areas (GG type baseline after Withers & Behrens, (1999)). Species concentrations determined using this baseline are in good agreement with NMR spectroscopic measurements for several alkali aluminosilicate compositions including Ab_{100} (Schmidt *et al*., 2001). The band at 4000 cm^{-1} is poorly resolved in the spectra of An and Di rich compositions. As a consequence, the gaussian fitted to this band is not well constrained and, therefore, determination of peak areas has a large uncertainty. On the other hand, determination of the peak heights after linear baseline subtraction shows always a very high reproducibility. Therefore, only peak heights were considered for quantifying water species and total water.

Table 3. Results of NIR spectroscopy.

composition	type of quench	total H_2O content (wt%)	density (g/l)	thickness (cm)	maximum H_2O-band (cm^{-1})	maximum OH-band (cm^{-1})	A_{H2O}	A_{OH}	C_{H2O} (wt%)	C_{OH} (wt%)	C_{water} (wt%)
Ab_{100}	RQ	2.29(15)	2352 [b]	0.0474	5219	4492	0.087	0.111	0.93(04)	1.41(07)	2.34(08)
Ab_{100}	NQ	2.46(15)	2350 [b]	0.0499	5224	4494	0.126	0.111	1.29(04)	1.35(07)	2.64(07)
Ab_{100}	NQ	5.99(22)	2301 [b]	0.0172	5223	4492	0.120	0.044	3.66(11)	1.58(13)	5.24(22)
Ab_{100}	RQ	6.41(10)	2294 [b]	0.0475	5223	4490	0.354	0.128	3.92(08)	1.66(08)	5.58(10)
$Ab_{50}An_{50}$	RQ	2.35(13)	2488 [b]	0.0476	5203	4487	0.039	0.118	0.65(08)	1.73(13)	2.38(10)
$Ab_{50}An_{50}$	NQ	2.67(17)	2483 [b]	0.0497	5204	4489	0.052	0.127	0.83(09)	1.78(13)	2.61(10)
$Ab_{50}An_{50}$	RQ	5.23(18)	2450 [b]	0.0472	5201	4483	0.168	0.171	2.88(26)	2.56(18)	5.44(11)
$Ab_{50}An_{50}$	NQ	5.81(21)	2457(20)	0.0416	5200	4489	0.169	0.139	3.27(30)	2.36(17)	5.63(13)
$Ab_{54}Di_{46}$ [a]	NQ	0.91(10)	2559(03)	0.0522	5206	4492	0.013	0.062	0.25(06)	0.68(05)	0.93(09)
$Ab_{54}Di_{46}$ [a]	NQ	0.99(10)	2559(03)	0.0524	5209	4489	0.013	0.063	0.25(06)	0.69(05)	0.94(09)
$Ab_{54}Di_{46}$ [a]	NQ	1.93(10)	2554(10)	0.0531	5211	4489	0.052	0.096	0.99(08)	1.04(07)	2.03(09)
$Ab_{54}Di_{46}$ [a]	NQ	1.95(11)	2554(10)	0.053	5214	4487	0.053	0.096	1.01(08)	1.04(07)	2.05(09)
$Ab_{54}Di_{46}$	RQ	2.04(13)	2543 [b]	0.0472	5209	4479	0.050	0.088	1.07(09)	1.07(07)	2.15(10)
$Ab_{54}Di_{46}$	NQ	2.55(14)	2534 [b]	0.0497	5211	4478	0.071	0.099	1.45(10)	1.15(08)	2.60(10)
$Ab_{54}Di_{46}$	NQ	4.94(15)	2488(35)	0.0182	5209	4475	0.057	0.044	3.24(26)	1.42(13)	4.66(28)
$Ab_{54}Di_{46}$	RQ	5.36(11)	2481 [b]	0.0485	5206	4474	0.196	0.117	4.19(25)	1.42(09)	5.62(12)
$An_{56}Di_{44}$ [a]	NQ	1.89(10)	2700(05)	0.0519	5175	4473	0.015	0.098	0.64(18)	1.22(11)	1.86(17)
$An_{56}Di_{44}$ [a]	NQ	1.99(13)	2700(05)	0.0522	5184	4468	0.019	0.101	0.81(21)	1.25(12)	2.06(17)
$An_{56}Di_{44}$	RQ	2.00(12)	2737(60)	0.0477	5187	4469	0.018	0.092	0.83(22)	1.23(12)	2.06(18)
$An_{56}Di_{44}$	NQ	2.23(21)	2670(38)	0.0494	5185	4468	0.022	0.106	1.00(24)	1.41(13)	2.41(18)
$An_{56}Di_{44}$	RQ	4.28(16)	2661 [b]	0.0482	5188	4467	0.068	0.152	3.18(65)	2.07(19)	5.26(19)
$An_{56}Di_{44}$	NQ	5.29(21)	2643 [b]	0.0187	5189	4467	0.029	0.051	3.52(80)	1.81(19)	5.33(48)

Notes: 2-5 spectra were averaged for each sample. The total water content is measured by KFT. Errors of KFT data given in parenthesis are based on an uncertainty of 0.02 µg/s in the titration rate. Estimated error is given for measured densities. Error in sample thickness is ± 2 µm. A = linear absorbance, error: ± 0.003. Error in the peak positions is ± 4 cm^{-1}.[a]) Samples were synthesised at 1250°C and 500 MPa for 24h, normal quench. [b]) calculated density. Errors in species concentrations and total water are calculated by error propagation. Note that the error in total water can be lower than that in the species concentrations because of opposing effects of the uncertainties in ε_{OH} and ε_{H_2O}. When ε_{OH} is underestimated then ε_{H_2O} will be overestimated.

4.3.3 Determination of molar absorption coefficients

Concentrations of water species in the glasses can be determined from the peak heights of the NIR bands using the Lambert-Beer-law

$$c_{H_2O} = \frac{1802 \cdot A_{H_2O}}{d \cdot \rho} \cdot \frac{1}{\varepsilon_{H_2O}} \qquad (4\text{-}5)$$

$$c_{OH} = \frac{1802 \cdot A_{OH}}{d \cdot \rho} \cdot \frac{1}{\varepsilon_{OH}} \qquad (4\text{-}6)$$

where A is the absorbance, d is the sample thickness (in cm), c_{H_2O} is the concentration of molecular H_2O (in wt%), c_{OH} is the concentration of water dissolved in form of OH-groups (in wt%), ρ is the density of the glass (in g/l) and ε is the linear molar absorption coefficient (in $l \cdot mol^{-1} \cdot cm^{-1}$). Assuming that there are no other water species besides H_2O and OH the total water content c_{water} is calculated as the sum of both species

$$c_{water} = c_{H_2O} + c_{OH} \qquad (4\text{-}7).$$

Inserting Eqn 4-5 and 4-4 into Eqn 4-7 and rearranging gives

$$\left(\frac{1802 \cdot A_{H_2O}}{d \cdot \rho \cdot c_{water}}\right) = \varepsilon_{H_2O} - \frac{\varepsilon_{H2O}}{\varepsilon_{OH}} \left(\frac{1802 \cdot A_{OH}}{d \cdot \rho \cdot c_{water}}\right) \qquad (4\text{-}8).$$

Eqn. 4-8 was used for the determination of the molar absorption coefficients by plotting the normalised absorbances (quotients in brackets) against each other. Provided that the molar absorption coefficients are independent of the total water content a straight line will be obtained. The assumption of concentration independent absorption coefficients is supported at least for water contents > 2 wt% by low temperature static NMR spectroscopy on alkali aluminosilicate glasses (Schmidt *et al.*, 2001). However, as shown by Zhang *et al.* (1997), the absorption coefficients for rhyolitic glasses with lower water concentrations may vary with the water content.

Molar absorption coefficients were determined by linear regressions for the glass compositions $Ab_{50}An_{50}$, $Ab_{54}Di_{46}$, and $An_{56}Di_{44}$ using the spectroscopic data given in Table 3. Glasses produced at 500 MPa were not considered in the calibration because such glasses loose easily water during preparation of IR sections.

The errors of the absorption coefficients are relatively high (standard deviations up to 9 % relative, see Table 4) because the number of samples and the variations in the A_{OH}/A_{H_2O} ratios are rather small. In particular the ε–values for the $An_{56}Di_{44}$ composition are poorly constrained because the two data points at low normalised OH absorbance (high total water contents) do not fall on a single line with the other data points (Fig. 3). The measured water content of the $An_{56}Di_{44}$ glass produced at

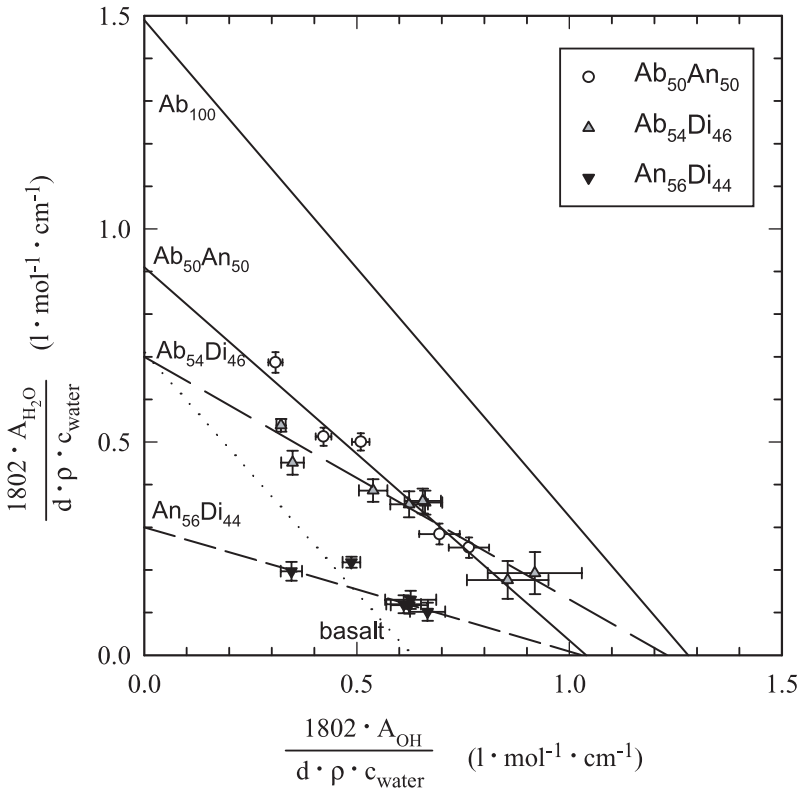

Fig. 3. Plot for determination of molar absorption coefficients for the OH combination bands at 4500 cm^{-1} and the H_2O combination band at 5200 cm^{-1}. Solid lines are for melts of the join Ab-An, dashed lines for Di-bearing melts. Lines based on data for Ab_{100} glasses (Behrens *et al.*, 1996) and for basaltic glasses (Ohlhorst *et al.*, 2001) are shown for comparison. The intercepts of the lines with the x and y axis correspond to the molar absorption coefficients for the OH and H_2O combination band, respectively.

1358°C/200 MPa is relatively low comparing to other data at 200 MPa and we suggest that the glass was not completely dehydrated during KFT (as mentioned above these glasses tend to explode during heating). In a preliminary evaluation of absorption coefficients we have, thus, not considered this sample. Using the spectroscopic data in (Table 3) and the absorption coefficients given in Table 4, the concentrations of OH groups and water molecules in the glasses were calculated (Fig. 4).

4.4 Water solubility

Water solubility data are listed in Table 2 and plotted in Fig. 5. A comprehensive data set of the solubility of H_2O in Ab melts in a wide range of pressures and temperatures is published elsewhere (Behrens, 1995; Behrens *et al.*, 2001). The data reported in this study are always based on experiments in which several compositions in the system Ab-An-Di were ran simultaneously.

With a few exceptions, IR spectroscopic water determinations of glasses are in good agreement with KFT measurements. We used KFT as the main method to constrain the water solubility in the melts because reliable IR calibrations could not be obtained for all compositions and because the precision of IR spectroscopy is relatively low for An and Di rich compositions due to low peak intensities. However, NIR spectroscopic data for Ab_{100} at

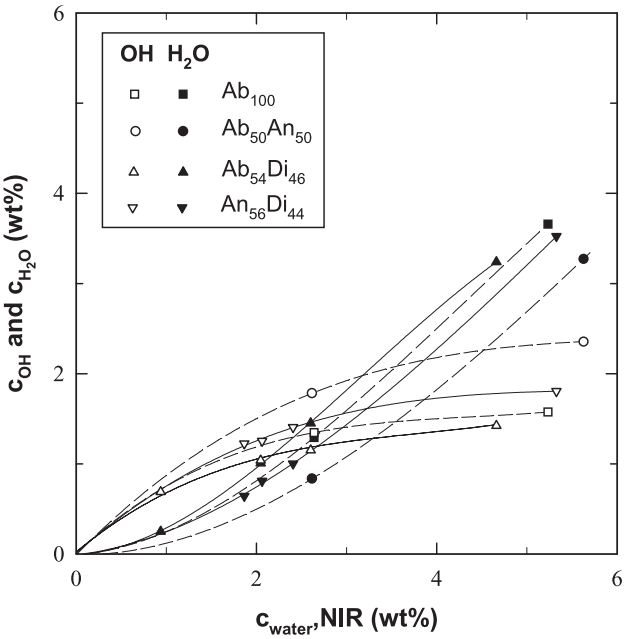

Fig. 4. Water speciation in glasses of the system Ab-An-Di. The cooling rate of all samples is close to 100°C/min near the glass transition. For errors see Table 3. Note the high concentrations of OH groups in the water-rich $Ab_{50}An_{50}$ glasses.

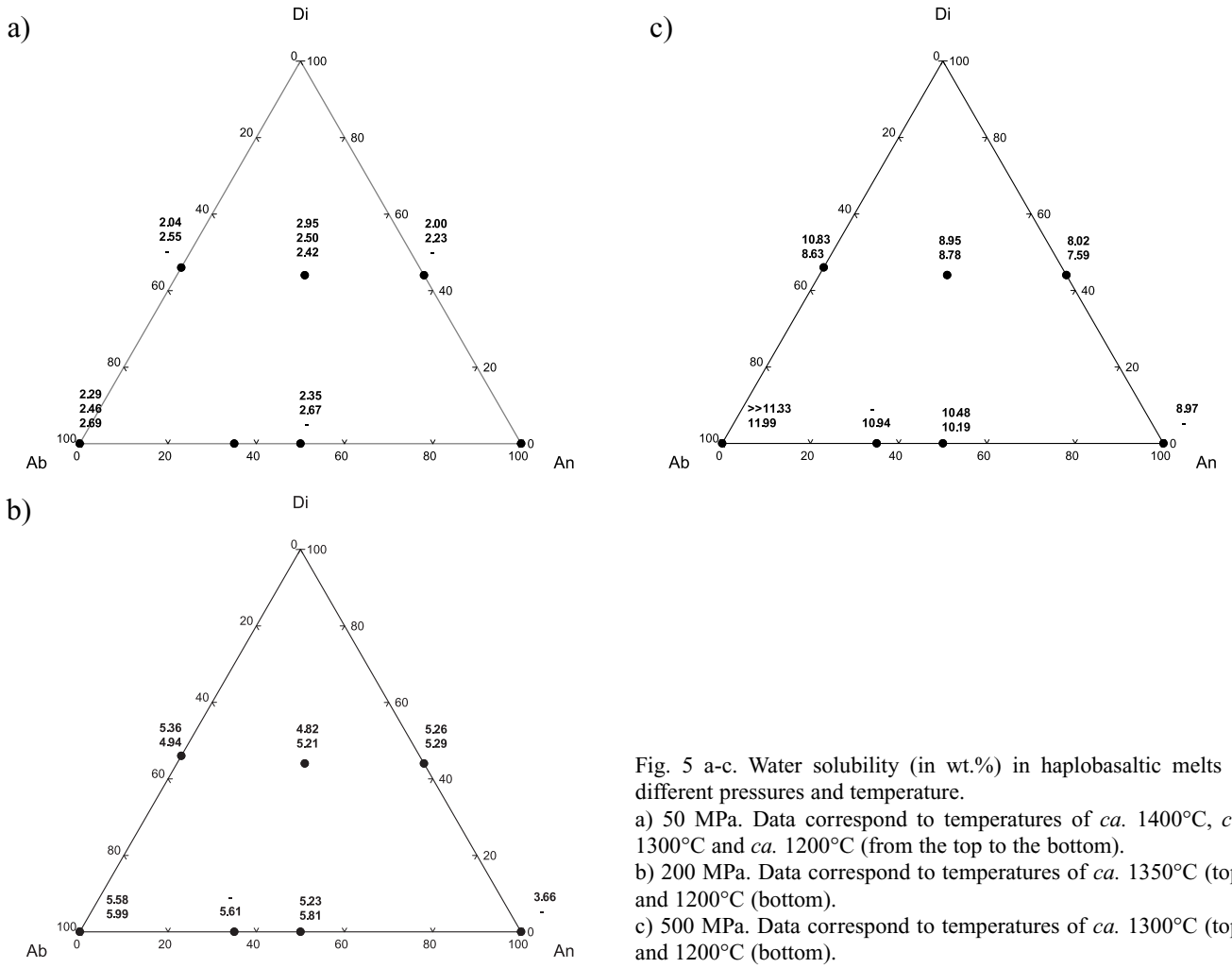

Fig. 5 a-c. Water solubility (in wt.%) in haplobasaltic melts at different pressures and temperature.
a) 50 MPa. Data correspond to temperatures of *ca.* 1400°C, *ca.* 1300°C and *ca.* 1200°C (from the top to the bottom).
b) 200 MPa. Data correspond to temperatures of *ca.* 1350°C (top) and 1200°C (bottom).
c) 500 MPa. Data correspond to temperatures of *ca.* 1300°C (top) and 1200°C (bottom).

1420°C/50 MPa (2.34 wt% water) and 1350°C/200 MPa (5.58 wt%) are in better agreement with trends derived by Behrens *et al.* (2001) and are favoured over the KFT values. Loss of water during KFT is indicated by NIR spectra for the $An_{56}Di_{44}$ glass produced at 1358°C/ 200 MPa.

5. Discussion

5.1 IR-spectroscopy

5.1.1 Variation of NIR absorption coefficients with composition

The molar absorption coefficients for both NIR combination bands decrease strongly with decreasing Ab content of the glass. This trend is evident at constant Di content as well as at constant An content (at least at low An contents), although data for intermediate compositions are looking to evaluate the trend in detail. The low absorption coefficients observed for natural basaltic compositions (Dixon *et al.*, 1995; Yamashita *et al.*, 1997; Ohlhorst *et al.*, 2001) are also consistent with this trend.

Adding Di component to glasses of the join Ab-An produces a strong decrease of the absorption coefficient for the H_2O combination band, *i.e.*, ε_{H_2O} is reduced from 1.49 $l \cdot mol^{-1} \cdot cm^{-1}$ for Ab_{100} to 0.70 $l \cdot mol^{-1} \cdot cm^{-1}$ for $Ab_{54}Di_{46}$. ε_{H_2O} further decrease with increasing An content of the glass to a value of 0.30 $l \cdot mol^{-1} \cdot cm^{-1}$ for the $An_{56}Di_{44}$ composition. This trend indicates that the excitation probability for the combination modes of H_2O molecules becomes very low in Di-rich melts. It appears that the change in the absorption coefficients is correlated to the shift in the positions of the peak maxima of the combination bands *i.e.* that peaks at lower wavenumber have lower absorption coefficients. However, as already noted for glasses with alkali feldspathic compositions (Behrens *et al.*, 1996), a simple relationship between peak position and ε values is not evident.

5.1.2 Water speciation in the glasses

The variation of species concentrations with total water content resembles that observed in other studies on silicate glasses (Silver *et al.*, 1990; Ohlhorst *et al.*, 2001). OH dominates at low c_{water} but with increasing c_{water} the relative abundance of H_2O molecules increases and the OH content

levels out (Fig. 4). The maximum concentrations of water dissolved as OH vary between 1.5 wt% ($Ab_{54}Di_{46}$) and 2.4 wt% ($Ab_{50}An_{50}$) in glasses quenched at a rate of ~ 100°C/min through the range of glass transition.

Faster quench yielded higher OH concentrations in Ab_{100}, $Ab_{50}An_{50}$ and $An_{56}Di_{44}$ glasses consistent with a higher fictive temperature of the glasses (Dingwell & Webb, 1990). Water speciation in the $Ab_{54}Di_{46}$ composition appears to be less sensitive to the cooling rate, which may indicate a strong temperature dependence of the viscosity near the glass transition for this particular composition. However, viscosity data are missing to prove this hypothesis. An explanation for the high concentration of OH groups in the $Ab_{50}An_{50}$ glass is that depolymerisation of the network structure by reaction of bridging oxygens with H_2O enables the formation of optimised coordination polyeder of the Ca cations. This idea is consistent with MAS-NMR spectroscopic observations showing that the environment of Na^+ in aluminosilicate glasses becomes more ordered upon hydration (Kohn *et al.*, 1998). In the case of Ca^{2+} we expect that local ordering in the environment of the cation is even more pronounced due to the higher charge of the cation compared to Na^+. However, it can not be ruled out that the variation in water speciation reflects simply variations in the glass transition temperature. For instance, $Ca_{0.5}AlSi_3O_8$ melts have much lower T_g than $NaAlSi_3O_8$ melts at same water content (Romano *et al.*, 2001). Viscosity data for hydrous plagioclase compositions are not available to clarify this point.

5.2 H_2O solubility in haplobasaltic melts

5.2.1 Effect of pressure and composition

The water solubility in haplobasaltic melts approximately doubles from 50 to 200 MPa and from 200 to 500 MPa: 2.5 to 5 to 10 wt% water. At 50 MPa 2.0-3.0 wt% water can be dissolved, 3.7-6.1 wt% at 200 MPa and 7.6-12.4 wt% at 500 MPa in the range of 1200-1420°C. At all P-T conditions, the lowest H_2O solubility was found in the $An_{56}Di_{44}$ melt. At 50 MPa, the variation of water solubility with composition appears to be complex (Fig. 5a). However, the variation in water solubility is small at 50 MPa compared to the experimental error and the precision of the data does not allow to extract reliably compositional trends. As shown in Fig. 5b and 5c, at 200 and 500 MPa the H_2O solubility in the melt decreases strongly with increasing Di content at constant An content (at least for Ab rich compositions). The pure An-Di system follows this trend at 500 MPa but not at 200 MPa. At 200 MPa, we found a significantly lower water solubility in the An_{100} melt (3.66 wt% at 1351°C) than in the $An_{56}Di_{44}$ melt (5.26 wt% at 1358°C). The water solubility in the An_{100} melt is relatively low compared to the other compositions of the join Ab-An at the same pressure. The result could not be verified at other temperatures because the liquidus for this composition at 200 MPa (1350°C, Yoder, 1965) is at the P-T limits of the experimental apparatus. The 200 MPa data show little variation of the H_2O solubility with the Ab/An ratio of the melt at constant Di content (Fig. 5b).

Table 4. Molar absorption coefficients for H_2O and OH combination bands.

Composition	SiO_2 (wt%)	range of H_2O (wt%)	ε_{OH} (l· mol^{-1}· cm^{-1})	ε_{H2O} (l· mol^{-1}· cm^{-1})
Ab_{100} [a]	69.19	0.5-9.2	1.28(5)	1.49(2)
$Ab_{50}An_{50}$	55.20	2.3-5.8	1.04(7)	0.91(8)
$Ab_{54}Di_{46}$	62.82	0.9-5.4	1.23(7)	0.70(4)
$An_{56}Di_{44}$	48.82	1.9-5.3	1.03(9)	0.30(6)
Basalt [b]	49.64	1.6-6.3	0.62(6)	0.71(8)

Notes: Absorption coefficients are given in terms of mole of H_2O component. Values in parenthesis are 1 σ errors in the last decimal. [a] Data for Ab_{100} from Behrens *et al.* (1996). [b] Data from Ohlhorst *et al.* (2001).

At 500 MPa, the effect of Ab/An ratio on dissolved water is much more pronounced than at lower pressures. At 1200°C, the H_2O solubility decreases along the Ab-An join from 11.99 wt% (Ab_{100}) to 10.94 wt% ($Ab_{65}An_{35}$) to 10.19 wt% ($Ab_{50}An_{50}$). The pure An_{100} composition is below its liquidus (1234°C at P_{H2O} = 500 MPa, Yoder, 1965) at this temperature but the low water solubility of 8.97 wt% observed at higher temperature (1320°C) indicates a further strong decrease in H_2O solubility towards higher An content. Along the nominal join $Ab_{50}Di_{50}$-$An_{50}Di_{50}$ a strong variation of the H_2O solubility with Ab/An ratio at 500 MPa is also evident. Our data indicate a decrease in the amount of dissolved water by 1.0 wt% at 1200°C and by 2.8 wt% at 1300-1310°C from the $Ab_{54}Di_{46}$ melt to the $An_{56}Di_{44}$ melt. The large difference at the higher temperature is mainly due to the strong increase in water solubility with temperature for the $Ab_{54}Di_{46}$ melt.

5.2.2 Effect of temperature

At 50 MPa the water solubility is found to decrease with increasing temperature for the following compositions: $An_{56}Di_{44}$, $Ab_{54}Di_{46}$, $Ab_{50}An_{50}$, Ab_{100} (Fig. 5a). At this pressure a negative T-dependence of the water solubility is observed also for haplogranitic and alkali feldspathic melt compositions (Holtz *et al.*, 1995; Behrens *et al.*, 2001). Such a T-dependence indicates a positive dissolution enthalpy for H_2O. The $Ab_{27}An_{29}Di_{44}$ melt shows a positive temperature dependence of water solubility, which increases from 2.42 wt% at 1200°C to 2.50 wt% at 1300°C to 2.95 wt% at ~ 1420°C. For the other compositions the variation in temperature is too small and there are not enough experiments to constrain any effect.

At 200 MPa a negative temperature dependence of water solubility is evident for Ab_{100}, $Ab_{50}An_{50}$, $Ab_{27}An_{29}Di_{44}$ and $An_{56}Di_{44}$. A different behaviour is observed for the $Ab_{54}Di_{46}$ melt. KFT data indicate an increase in the solubility of H_2O from 4.94 wt% at 1200°C to 5.36 wt% at 1358°C. IR spectroscopy confirms the higher water content in the glass produced at higher temperature.

At 500 MPa an increase in the H_2O solubility with increasing temperature is evident from the KFT measurements for all melt compositions, except for Ab_{100}. However, large amounts of micrometer size bubbles in

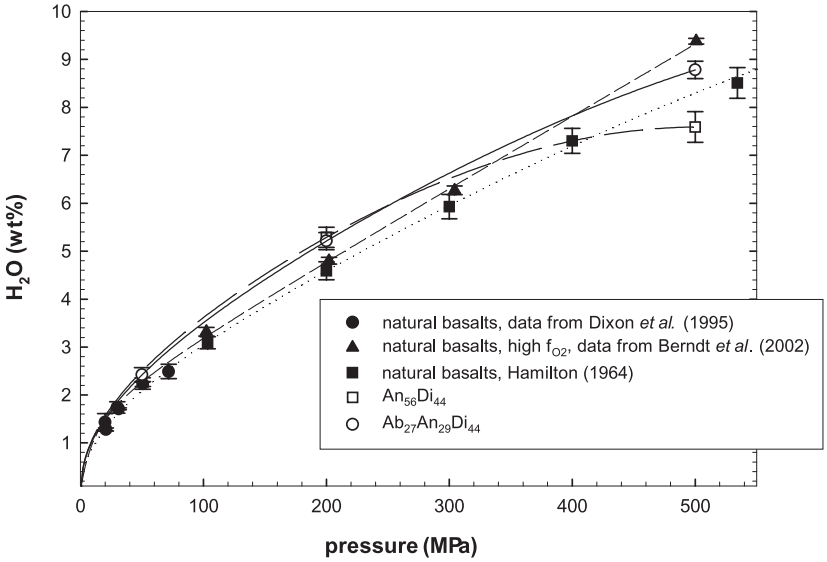

Fig. 6. Variation of water solubility with pressure at 1200°C. Data for natural basalt melts from Berndt *et al.* (2002), Dixon *et al.* (1995) and Hamilton (1964) are shown for comparison. Solid line-$Ab_{27}An_{29}Di_{44}$ melt (this study), long dashed line-$An_{56}Di_{44}$ melt (this study), short dashed line-natural basaltic melts at high fO_2 from Berndt *et al.* (2002), dotted line-natural basalt melts determined by Hamilton (1964).

glasses quenched rapidly from temperatures 1300-1330°C indicate a large positive T-dependence of water solubility in Ab_{100} melts at least at high temperature. The KFT analysis yields a water content significantly lower than that expected from experiments at lower temperature (Behrens *et al.*, 2001) and we infer that the amount of water exsolved during cooling was too large to be preserved in the glass as bubbles. The $An_{56}Di_{44}$ glass produced at 1300°C/500 MPa contained only few large elongated bubbles mainly near its surface. The shape and distribution of the bubbles differ from typical quench bubbles which are usually homogeneously distributed in the glass, with spherical shapes and diameters of 10 μm. We suggest that these bubbles were formed by fluid-melt mingling rather than by H_2O exsolution upon quench. $Ab_{50}An_{50}$ melts were quenched to clear, bubble-free glasses at 500 MPa from temperatures of 1200-1320°C both at slow and rapid quenches. This indicates that the water solubility in this melt does not increase significantly with temperature at 500 MPa.

5.3 Comparison with other studies

A first estimate for the solubility of water in melts of the system Ab-An-Di was given by Yoder (1965). The value of about 8.8 wt% for the eutectic melt composition ($An_{73}Di_{27}$) of the binary join An-Di at 1095°C/500 MPa is in good agreement with our data for An rich melts ($An_{56}Di_{44}$: 7.59 wt% at 1200°C and 8.02 wt% at 1300°C; An_{100}: 8.97 wt% at 1320°C). The study of Oxtoby & Hamilton (1978) on water solubility in plagioclase melts suffers from experimental and analytical problems (Behrens, 1995; Holtz *et al.*, 1995). Their data at pressures above 400 MPa are not reliable because the glasses lost already water during drying before water determination using the weight loss method, *i.e.* the Ab-rich glasses. At 1200°C, 200 MPa we found systematically lower H_2O solubilities than Oxtoby & Hamilton (1978). A possible explanation is that these authors have used glass powders as starting materials and initially trapped water bubbles were not removed during the run due to high melt viscosities.

Results of older studies on water solubility in natural basaltic melts are difficult to interpret due to experimental problems. In the experiments of Khitarov *et al.* (1968) on basalt extruded from the Klyuchevskava Sopka volcano quench phases were observed in the run products and the redox state of the melt was unknown. Nevertheless, their H_2O solubility value of 8.5 wt.% obtained at 1200°C/500 MPa is in good agreement with our determinations for An and Di rich melts ($Ab_{27}An_{29}Di_{44}$: 8.78 wt%, $An_{56}Di_{44}$: 7.59 wt%). At lower pressure, however, these authors report significant lower water solubilities than measured in our study.

Recently, Berndt *et al.* (2002) investigated the water solubility in a primitive MORB composition at 1200°C and pressures from 50 to 500 MPa using a similar rapid quench device as in our study. Two different fO_2 were investigated either close to MnO-Mn_3O_4 or near the QFM buffer conditions. At 50 and 200 MPa their water solubility data (2.14-2.28 wt% and 4.46-4.80 wt%, respectively, depending on fO_2 are lower than our values for haplobasaltic melts (Fig. 6). On the other hand, at 500 MPa the H_2O solubility in the natural basaltic melt is higher (9.38 wt%) than in our Di and An rich melts. The differences might be due to compositional effects. In particular dissolved iron (not present in the haplobasalt) may have a strong influence on water solubility. As noted by Berndt *et al.* (2002), the measurements of Hamilton *et al.* (1964) tend to underestimate the solubility of H_2O in basaltic melts at high pressure due to problems related with the weight loss method used for measuring water contents in quenched glasses. At pressures up to

200 MPa, H_2O solubility data for basalt melts from Hamilton *et al.* (1964), Dixon *et al.* (1995) and Berndt *et al.* (2002) are in good agreement. Slight differences between these data may be explained by variations in composition (as indicated in our study) and in oxygen fugacity.

5.4 Comparison to tonalitic melts - Implications for the dissolution mechanism of H_2O in silicate melts

In the haplotonalite system Qz-Ab-An at 1200°C, Grams & Behrens (1996) found an increase of water solubility with increasing An content of the melt at 50 MPa. This trend reverses at 500 MPa with the highest H_2O solubility in the pure Ab melt. Our measurements at 500 MPa are consistent with these results in that increasing the alkaline earth content of the melt reduces the water solubility. The trend at 50 MPa could not be verified for the system Ab-An-Di due to the analytical uncertainties.

The change of the water solubility in polymerised melts (system Qz-Ab-An) with increasing An content can be rationalised by the influence of Ca^{2+} on the melt structure. Ca^{2+} has a similar ion radius as Na^+ (Ca^{2+} = 0.99 Å, Na^+ = 0.95Å) but a double positive charge. Thus, the silicate network becomes more contracted as Na^+ is substituted by Ca^{2+}. At high pressure (high water content) this effect leads to a decrease in the water solubility due to a decrease in free volume. On the other hand, at low pressure (low water content) the effect of melt depolymerisation due to formation of OH groups by reaction of H_2O with bridging oxygen appears to be dominant. The depolymerisation of the network facilitates the formation of optimised coordination polyeders of alkaline earth cations, *i.e.* cation-oxygen distances and bonding angles can be adjusted to minimise the Gibbs-free energy. It is noteworthy that these polyeders do not necessarily contain hydrous species (OH, H_2O) beside network oxygens.

In haplobasaltic melts the network is already depolymerised due to the presence of the Di component. Hence, reduction of the Gibbs-free energy of the melt by complexation of cations is not a driving force for water incorporation at low pressure. The optimised coordination of cations to oxygen can be adjusted by non-bridging oxygens already present in the water-free melt. Hence, at all pressures the contracting effect of divalent cations on melt structure, reducing the free volume in the melt, is dominating in haplobasaltic melts.

5.5 Implications for magma genesis and evolution

According to our results at most 5 wt% of water can be dissolved in basaltic melts at 200 MPa. Hence, to produce a fraction of ~ 20 vol% of water saturated melt in a basaltic rock a bulk water content of only 1 wt% is necessary. At 200 MPa such a melt fraction can be achieved in MOR basalt already at temperatures just above 1000°C (Berndt, 2002). At more shallow depths (lower pressure) the amount of water required to generate the same melt fraction is even lower due to the lower water solubility.

Even primitive MORB melts of mid-ocean ridge environments may contain low but significant water contents: from ~ 0.1-0.2 wt% for N- and T-MORB, (Sobolev & Chaussidon, 1996) up to ~ 1.5 wt% (Kamenetsky *et al*., 2000). If the magma chamber replenishment is hampered, the water content of the melt increases strongly during differentiation of the magma. The increase in melt water content is caused by the decrease in melt fraction, the enrichment of sodium feldspar component in the melt and the negative temperature dependence of water solubility at pressures up to 200 MPa.

6. Conclusions

New water solubility data are presented for melts with compositions along the nominal joins Ab-An and $Ab_{50}Di_{50}$-$An_{50}Di_{50}$. Our results show that increasing the Di content of the melt decreases strongly the water solubility (especially at 500 MPa). The effect of the Ab/An ratio on water solubility depends on pressure and Di content (degree of polymerisation) of the melt. At 500 MPa the solubility of H_2O drops strongly with decreasing Ab/An ratio for both binary joins. At pressures 50-200 MPa the Ab/An ratio has only a minor influence on water solubility, except possibly for very An-rich melts of the join Ab-An. Compared to natural basaltic melts the pressure dependence of the H_2O solubility appears to be more pronounced in Di and An rich haplobasaltic melts at low pressures but less pronounced at high pressure. These observations are attributed to differences in structural properties of Fe^{2+} and Fe^{3+} (present in natural basalts) compared to their substitutes in haplobasaltic melts (Mg^{2+}, Ca^{2+} and Al^{3+}).

Acknowledgment: We acknowledge support of the study by the German DFG. We thank Matthias Grams and Martin Meyer for performing some of the solubility experiments. Helpful comments of Jürgen Koepke are acknowledged.

References

Behrens, H. (1995): Determination of water solubilities in high-viscosity melts: An experimental study on $NaAlSi_3O_8$ and $KalSi_3O_8$ melts. *Eur. J. Mineral.*, **7**, 905-920.

Behrens, H., Romano, C., Nowak M., Holtz F., Dingwell, D.B. (1996): Near infrared spectroscopic determination of water species in glasses of the system $MAlSi_3O_8$ (M = Li, Na, K): an interlaboratory study. *Chemical Geol.*, **128**, 41-63.

Behrens, H., Meyer, M., Holtz, F., Benne, D., Nowak, M. (2001): The effect of alkali ionic radius, temperature, and pressure on the solubility of water in $MAlSi_3O_8$ melts (M = Li, Na, K, Rb). *Chemical Geol.*, **174**, 275-289.

Berndt, J. (2002): Differentiation of MOR basalt at 200 MPa: Experimental techniques and influence of H_2O and fO_2 on phase relations and liquid line of descent. PhD thesis, Hannover, 118 p.

Berndt, J., Liebske, C., Holtz, F., Freise, M., Nowak, M., Ziegenbein, D., Hurkuck, W., Koepke, J. (2002): A combined rapid-quench and H_2-membrane setup for internally heated pressure vessels: Description and application for water solubility in basaltic melts. *Am. Mineral.*, **87**, 1717-1726.

Boudier, F., Godard, M., Armbruster, C., (2000): Significance of gabbronorite occurrence in the crustal section of the Semail ophiolite. *Marine Geophys. Res.*, **21**, 307-326.

Burnham, C.W. & Jahns, R.H. (1962): A method for determining the solubility of water in silicate melts. *Am. J. Sci.*, **260**, 721-745.

Dingwell, D.B. & Webb, S.L. (1990): Relaxation in silicate melts. *Eur. J. Mineral.*, **2**, 427-449.

Dixon, J.E., Stolper, E.M., Holloway, J.R. (1995): An experimental study of water and carbon dioxide solubilities in mid-ocean ridge basaltic liquids; Part I: Calibration and solubility models. *J. Petrol.*, **36**, 1607-1631.

Grams, M. & Behrens, H. (1996): Water solubility in tonalitic melts. *TERRA abstracts*, **8**, 23.

Hamilton, D.L., Burnham, C.W., Osborn, E.F. (1964): The solubility of water and effects of oxygen fugacity and water content on crystallization in mafic magmas. *J. Petrol.*, **5**, 21-39.

Holtz, F., Behrens, H., Dingwell, D.B., Johannes, W. (1995): H_2O solubility in haplogranitic melts; compositional, pressure and temperature dependence. *Am. Mineral.*, **80**, 94-108.

Johannes, W. & Holtz, F. (1996): Petrogenesis and experimental petrology of granitic rocks. Minerals and Rocks 22, Springer Verlag, Berlin, 335 p.

Kamenetsky, V.S., Everard, J.L., Crawford, A.J., Varne, R., Eggins, S.M., Lanyon, R. (2000): Enriched end-member of primitive MORB melts: petrology and geochemistry of glasses from Macquarie Island (SW Pacific). *J. Petrol.*, **41**, 411-430.

Khitarov, N. I., Kadik, A.A., Lebedev, E. B. (1968): Solubility of water in a basalt melt. *Geokhimia*, **7**, 763-772.

Kohn, S.C., Smith, M.E., Dirken, P.J., van Eck, E.R.H., Kentgens, A.P.M., Dupree, R. (1998): Sodium environments in dry and hydrous albite glasses; Improved ^{23}Na solid state NMR data and their implications for water dissolution mechanisms. *Geochim. Cosmochim. Acta*, **62**, 79-87.

Morse, S.A., (1980): Basalts and phase diagrams. *in "*An introduction to the quantitative use of phase diagrams in igneous petrology". Springer Verlag, 37-58 and 77-84.

Nowak, M. & Behrens, H. (1995): The speciation of water in haplogranitic glasses and melts determined by *in situ* near-infrared spectroscopy. *Geochim. Cosmochim. Acta*., **59**, 3445-3450.

—, — (2001): Water in rhyolitic magmas: getting a grip on a slippery problem. *Earth Planet. Sci. Letters*, **184**, 515-522.

Ohlhorst, S., Behrens, H., Holtz, F. (2001): Compositional dependence of molar absorptivities of near-infrared OH- and H_2O bands in rhyolitic to basaltic glasses. *Chemical Geol.,* **174**, 5-20.

Oxtoby, S. & Hamilton, D.L. (1978). Water in plagioclase melts. In: Progress in experimental petrology; fourth progress report of research supported by N.E.R.C., 1975-1978, ed. W.S. Mackenzie, *Nat. Environ. Res. Council Publ. Series D*, Department of Geology, Manchester University, **11**, 36-37.

Romano, C., Poe, B., Mincione, V., Hess, K.U., Dingwell, D.B. (2001): The viscosities of dry and hydrous $xAlSi_3O_8$ (x = Li, Na, K, $Ca_{0.5}$, $Mg_{0.5}$) melts. *Chemical Geol.*, **174**, 115-132.

Richet, P., Whittington, A., Holtz, F., Behrens, H., Ohlhorst, S., Wilke, M. (2000): Water and the density of silicate glasses. *Contrib. Mineral. Petrol.*, **138**, 337-347.

Roux, J. & Lefèvre, A. (1992): A fast quench device for internally heated pressure vessels. *Eur. J. Mineral.*, **4**, 279-281.

Schmidt, B.C., Behrens, H., Riemer, T., Kappes, R., Dupree, R. (2001): Quantitative determination of water speciation in aluminosilicate glasses: a comparative NMR and IR spectroscopic study. *Chemical Geol.*, **174**, 195-208.

Scholze, H. (1960): Zur Frage der Unterscheidung zwischen H_2O-Molekeln und OH-Gruppen in Gläsern und Mineralen. *Naturwissenschaften*, **47**, 226-227 (in German).

Silver, L.A., Ihinger, P.D., Stolper, E. (1990): The influence of bulk composition on the speciation of water in silicate glasses. *Contrib. Mineral. Petrol.*, **104**, 142-162.

Shen, A.H. & Keppler, H. (1995): Infrared spectroscopy of hydrous silicate melts to 1000 degrees C and 10 kbar; direct observation of H_2O speciation in a diamond-anvinl cell. *Am. Mineral.*, **80**, 1335-1338.

Sobolev, A.V. & Chaussidon, M. (1996): H_2O concentrations in primary melts from supra-subduction zones and mid-ocean ridges; implications for H_2O storage and recycling in the mantle. *Earth Planet. Sci. Lett.*, **137**, 45-55.

Stolper, E. (1982): Water in silicate glasses; an infrared spectroscopic study. *Contrib. Mineral. Petrol.*, **81**, 1-17.

Webster, J.D., Kinzler, R.J., Mathez, E.A. (1999): Chloride and water solubility in basalt and andesite melts and implications for magmatic degassing. *Geochim. Cosmochim. Acta*, **63**, 729-738.

Withers, A.C. & Behrens, H. (1999): Temperature induced changes in the NIR spectra of hydrous albitic and rhyolitic glasses between 300 and 100 K. *Phys. Chem. Minerals*, **27**, 119-132.

Yamashita, S., Kitamura, T., Kusakabe, M. (1997): Infrared spectroscopy of hydrous glasses of arc magma compositions. *Geochem. J.*, **31**, 169-174.

Yoder, H.S. (1965): Diopside-anorthite-water at five and ten kilobars and its bearing on explosive volcanism. *Yrbk. Carnegie Inst. Wash.*, 82-89.

Zhang, Y., Belcher, R., Ihinger, P.D., Wang, L.P., Xu, Z.J., Newman, S. (1997): New calibration of infrared measurement of dissolved water in rhyolitic glasses. *Geochim. Cosmochim. Acta*, **61**, 3089-3100.

Zhang, Y., Xu, Z., Behrens, H. (2000): Hydrous species geospeedometer in rhyolite: improved calibration and application. *Geochim. Cosmochim. Acta*, **64**, 3347-3355.

Received 12 June 2002
Modified version received 18 February 2003
Accepted 24 March 2003